

Spin relaxation in hydrogenated graphene

M. R. Thomsen,^{1,2} M. M. Ervasti,³ A. Harju,³ and T. G. Pedersen^{1,2}

¹*Department of Physics and Nanotechnology, Aalborg University, DK-9220 Aalborg Øst, Denmark*

²*Center for Nanostructured Graphene (CNG), DK-9220 Aalborg Øst, Denmark*

³*COMP Centre of Excellence, Department of Applied Physics, Aalto University, Helsinki, Finland*

(Received 17 July 2015; revised manuscript received 3 September 2015; published 9 November 2015)

We calculate the spin transport of hydrogenated graphene using the Landauer-Büttiker formalism with a spin-dependent tight-binding Hamiltonian. Hydrogen adatoms are a common defect and they carry a finite magnetic moment, which makes it important to understand their influence on spin transport for graphene-based spin devices. Our tight-binding model accurately reproduces the density-functional theory band structure and atom-projected density of states. The advantages of using the Landauer-Büttiker formalism are that it simultaneously gives information on sheet resistance and localization length as well as spin relaxation length. Furthermore, the transport can be computed very efficiently using this method by employing the recursive Green's function technique. Here, we study hydrogen adatoms on graphene with randomly aligned magnetic moments, where interference effects are explicitly included. We show that a 5 ppm hydrogen defect density is sufficient to reduce the spin relaxation length to 2 μm and that the inverse spin relaxation length and sheet resistance scale nearly linearly with the impurity concentration. Moreover, the spin relaxation mechanism in hydrogenated graphene is Markovian only near the charge neutrality point or in the highly dilute impurity limit.

DOI: [10.1103/PhysRevB.92.195408](https://doi.org/10.1103/PhysRevB.92.195408)

PACS number(s): 72.25.-b, 72.10.Fk, 72.80.Vp

I. INTRODUCTION

Spin transport in graphene has attracted a lot of attention in recent years due to very long spin relaxation times and spin relaxation lengths predicted for this material [1,2]. The spin relaxation length in graphene has been predicted theoretically to be at least 20 μm [1] for experimentally realistic device parameters, whereas experimental values are about an order of magnitude lower, typically around 1–4 μm [3–8], but has been observed as large as around 200 μm in short samples at low temperature [9] and 12 μm in encapsulated graphene at room temperature [10]. It has been ruled out experimentally that this discrepancy is due to hyperfine interactions with the naturally occurring ^{13}C isotope in graphene [7]. Experimental measurements of graphene in the presence of a strong magnetic field show that the observed low spin relaxation length is, at least in part, due to magnetic impurities in graphene [11]. Magnetic impurities are very common in graphene and may, for instance, be hydrogen adatoms [12], vacancies [12,13], or embedded metal atoms [14,15] in graphene pores. An attempt to explain the effects of magnetic impurities in graphene has been given by Kochan *et al.* [16]. They find that 0.36 ppm coverage of hydrogen adatoms is sufficient to obtain spin relaxation times that are in agreement with experiments. Their model is based on the Green's function of a single hydrogen adatom in an infinite graphene sheet and multiplying the results with the impurity concentration. In effect, their model does not include interference effects between scatterers and is thus only valid in the highly dilute limit. Spin transport in hydrogenated graphene was also considered by Soriano *et al.* [17,18]. Their method is based on a mean-field Hubbard Hamiltonian and the real space Kubo-transport formalism. They find that a coverage of 15 ppm hydrogen adatoms gives the correct order of magnitude of the spin relaxation time [18], which is more than an order of magnitude larger than the prediction by Kochan *et al.* Additionally, the energy dependence of the two theoretical predictions for the spin relaxation time do not agree

with the experimental findings. A recent *ab initio* study of the spin scattering of hydrogen adatoms on narrow armchair graphene nanoribbons by Wilhelm *et al.* [19] has shown that spin scattering off a single hydrogen adatom with defect spin oriented perpendicular to the electron spin is sufficient to obtain spin-flip conductance on the same order of magnitude as the spin-conserved conductance. They also showed spin-orbit interactions to be negligible compared to exchange interactions in the context of spin scattering on hydrogen adatoms.

The spin relaxation length is determined by the decay rate of spin polarization. Zurek *et al.* [20] have found through a phenomenological spin interaction Hamiltonian that the spin relaxation decay rate depends on the distribution of coupling strengths between a spin system and an environment with many independent spins. In particular, they find that a Gaussian distribution of couplings leads to Gaussian decay of the spin polarization with respect to time, whereas a Lorentzian distribution leads to exponential decay. It is straightforward to demonstrate that the spin relaxation of scatterers on a classical Markovian chain is also exponential. Therefore, the exponential decay of spin polarization is typically referred to as Markovian behavior [21].

In this paper, we calculate the spin-dependent electron transport on graphene with hydrogen adatoms using the Landauer-Büttiker formalism, which is a widely used method for calculating quantum transport in nanoscale devices [19,22–27]. We use hydrogen adatoms as they are very common magnetic defects on graphene. Each defect has a finite magnetic moment of $1\mu_B$. Additionally, due to local sp^3 hybridization, heavily hydrogenated graphene has an energy gap [28]. In particular, we will demonstrate that the Landauer-Büttiker formalism can be used to extract the spin relaxation length of a system. We will demonstrate that the spin relaxation is not always Markovian and that inverse spin relaxation length and sheet resistance scale nearly linearly with impurity concentration.

II. THEORETICAL METHODS

We start by simulating a hydrogen adatom on graphene in a supercell geometry using density-functional theory (DFT) as implemented in the FHI-AIMS package [29]. It is an all-electron code with numerical atom-centered basis functions. We use the default *tight* basis set for each atom type in a spin-polarized calculation. The electron-electron interactions are treated at the level of the Perdew-Burke-Ernzerhof (PBE) exchange-correlation functional [30]. The hydrogen adatom on graphene is relaxed in a supercell with $2 \times 8 \times 8 = 128$ carbon atoms, until the forces between the atoms are smaller than 10^{-3} eV/Å. We expect the supercell to be large enough for finite size effects to be negligible to describe hydrogen adatoms in the dilute limit. Moreover, the DFT self-consistency cycle is considered converged if, among other things, the total energy changes by less than 10^{-6} eV. We use an $8 \times 8 \times 1$ k -point Monkhorst-Pack grid during relaxation. The final band structure and density of states (DOS) calculations use Γ -centered grids of $15 \times 15 \times 1$ k points, whereas the atom-projected partial DOS (PDOS) calculation uses a grid of $12 \times 12 \times 1$ k points.

The DFT band structure, DOS, and PDOS of a system with a hydrogen adatom are shown in Fig. 1. There are spin-polarized impurity bands on both sides of the Fermi energy that also appear as peaks in the total DOS. The occupied impurity band of the majority spin component results in a spin moment of $1.0\mu_B$. The states corresponding to the impurity band, and the resulting spin density thereof, are localized at the hydrogen atom (H) and at the sublattice neighboring the carbon atom (C_0) underneath the hydrogen atom. Other models, such as Ref. [17], remove the H and C_0 atom sites, such that the vacancy in the lattice results in a similar spin density profile.

We fit tight-binding (TB) models to the DFT band structures and PDOS in order to simulate systems with a large number of hydrogen adatoms in the dilute limit. We start with a tight-binding model of graphene, written as

$$\hat{H}_0 = \sum_{i,j} t_{ij} |i\rangle \langle j|, \quad (1)$$

where $|i\rangle$ is a state localized at the lattice site i , and t_{ij} are hopping parameters between the lattice sites. The carbon on-site energy is taken as the energy zero point. We take hoppings up to third-nearest neighbors, and we denote the first-, second- and third-nearest-neighbor hopping elements as t_1 , t_2 , and t_3 , respectively. By fitting to the pristine graphene DFT band structure, we find the C-C hopping parameters $t_1 = -2.855$ eV, $t_2 = -0.185$ eV, and $t_3 = -0.190$ eV. The t_1 and t_2 parameters are fitted freely, and t_3 is included by assuming that $t_3 = t_1(0.18/2.7)$, where the factor is motivated by earlier models [31].

It turns out that the systems with a hydrogen adatom can be accurately described with remarkably simple models, at least in the dilute limit. Namely, we introduce a new site corresponding to the hydrogen adatom (H), and we couple it to the graphene backbone by allowing only a spin-independent hopping t' to the carbon site beneath it (C_0). Moreover, the hydrogen on-site potential is taken as spin dependent with values of ε_\uparrow and ε_\downarrow for the majority and minority spin channels, respectively. The model Hamiltonian in the case of a single

hydrogen adatom is written as

$$\begin{aligned} \hat{H} = & \hat{H}_0 + t'(|C_0\rangle \langle H| + |H\rangle \langle C_0|) \\ & + |H\rangle \langle H| \otimes (\varepsilon_\uparrow |\uparrow_{\mathbf{a}}\rangle \langle \uparrow_{\mathbf{a}}| + \varepsilon_\downarrow |\downarrow_{\mathbf{a}}\rangle \langle \downarrow_{\mathbf{a}}|), \end{aligned} \quad (2)$$

where the spin-independent parts are shortened as $\hat{H}_0 \otimes \mathbb{1} = \hat{H}_0$, and $|\uparrow_{\mathbf{a}}\rangle$ and $|\downarrow_{\mathbf{a}}\rangle$ are the orthogonal spin basis vectors along the spin-quantization axis $\mathbf{a} = (\sin\theta \cos\phi, \sin\theta \sin\phi, \cos\theta)$, such that $|\uparrow_{\mathbf{a}}\rangle = \cos(\theta/2)|\uparrow\rangle + e^{i\phi} \sin(\theta/2)|\downarrow\rangle$ and $|\downarrow_{\mathbf{a}}\rangle = e^{-i\phi} \sin(\theta/2)|\uparrow\rangle - \cos(\theta/2)|\downarrow\rangle$, where we have used the shorthand notation $|\uparrow\rangle = |\uparrow_{\hat{z}}\rangle$ and $|\downarrow\rangle = |\downarrow_{\hat{z}}\rangle$. The spin-quantization axis for the charge carriers is chosen to be \hat{z} in all calculations.

We fit the tight-binding model to the DFT band structure and PDOS. Specifically, we compare the six lowest unoccupied and six highest occupied bands, and fit the two-dimensional band energies in the first Brillouin zone. The DFT PDOS is fitted to the TB local DOS (LDOS) in the defect neighborhood up to the fourth-nearest carbon atoms surrounding the hydrogen adatom. We find that the C-H hopping is $t' = 9.475$ eV, and the hydrogen on-site potentials have values $\varepsilon_\uparrow = 1.853$ eV for the majority spin component and $\varepsilon_\downarrow = 4.689$ eV for the minority spin component. The fitted TB band structure, total DOS, and LDOS are shown in Fig. 1, where they are compared to the DFT calculations. The figure shows excellent agreement between the TB model and the DFT results. One should note that the model parameters depend slightly on the number of energy bands and PDOS atoms, and the corresponding weights for these in the cost function, but this will only have a marginal effect on the obtained results.

We consider the quantization axis of the defect spin moments as classical vectors that can be rotated individually, and eventually ensemble average results over different rotation angles and defect position realizations. To do this, we write the spin-dependent part of the model Hamiltonian, Eq. (2), as

$$\varepsilon_\uparrow |\uparrow_{\mathbf{a}}\rangle \langle \uparrow_{\mathbf{a}}| + \varepsilon_\downarrow |\downarrow_{\mathbf{a}}\rangle \langle \downarrow_{\mathbf{a}}| = \frac{\varepsilon_\uparrow + \varepsilon_\downarrow}{2} \mathbb{1} + \frac{\varepsilon_\uparrow - \varepsilon_\downarrow}{2} \hat{\sigma}_{\mathbf{a}}, \quad (3)$$

where $\mathbb{1} = |\uparrow_{\mathbf{a}}\rangle \langle \uparrow_{\mathbf{a}}| + |\downarrow_{\mathbf{a}}\rangle \langle \downarrow_{\mathbf{a}}|$ is the identity matrix and $\hat{\sigma}_{\mathbf{a}} = |\uparrow_{\mathbf{a}}\rangle \langle \uparrow_{\mathbf{a}}| - |\downarrow_{\mathbf{a}}\rangle \langle \downarrow_{\mathbf{a}}|$ is the Pauli z matrix in the given basis. For each defect, we define the rotation angles θ and ϕ on the Bloch sphere. As the only spin-dependent parameter is the hydrogen on-site potential, spin flipping only occurs at these sites when the charge carrier spin is not aligned with the defect spin. In the $\{|\uparrow\rangle, |\downarrow\rangle\}$ basis, $\hat{\sigma}_{\mathbf{a}}$ is given by

$$\begin{aligned} \hat{\sigma}_{\mathbf{a}} = & \cos\theta |\uparrow\rangle \langle \uparrow| - \cos\theta |\downarrow\rangle \langle \downarrow| \\ & + e^{-i\phi} \sin\theta |\uparrow\rangle \langle \downarrow| + e^{i\phi} \sin\theta |\downarrow\rangle \langle \uparrow|. \end{aligned} \quad (4)$$

The rotation of the defect spins is similar to the method used in Ref. [19], except that we rotate each defect spin individually. The reasons why we do this are the following: In the dilute limit, the interactions between the defects can be assumed small. Then a finite temperature or other environmental factors, e.g., local Zeeman terms originating from the graphene curvature or substrate, can break the magnetic ordering in a system with many hydrogen adatoms. In such a case, we cannot choose the same spin basis simultaneously for all the defect spin moments. Instead, the defect spin moments can be at least partly uncorrelated, pointing to somewhat random directions. On the other hand, in the limit of many

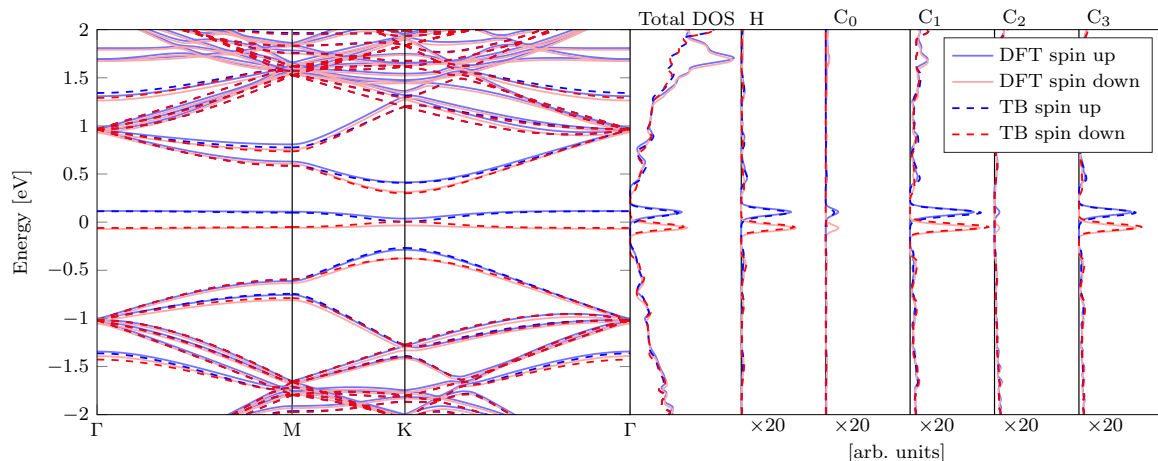


FIG. 1. (Color online) Spin-polarized band structure, total DOS, and PDOS of an 8×8 supercell with a hydrogen adatom for both the majority and minority spin components. The DFT PDOS is compared to the TB LDOS at the hydrogen atom (H), the carbon atom underneath the hydrogen atom (C_0), and its first-, second-, and third-nearest neighbors C_1 , C_2 , and C_3 , respectively.

nearby defects, frustration can result in a nontrivial defect spin moment configuration that can be difficult to estimate without explicitly including the defect spin-spin interactions.

The transmittance between any two leads p and q of a multiterminal system can be calculated using the Landauer-Büttiker formula [24] $T_{pq} = \text{Tr}\{\Gamma_p G \Gamma_q G^\dagger\}$, where $G = [(E + i\varepsilon)I - H - \sum_n \Sigma_n]^{-1}$ is the retarded Green's function. Σ_n and Γ_n are the self-energy and linewidth functions, respectively, of lead n . The leads are modeled here as pristine graphene ribbons with the same unit cell width as the device region and the electronic transport is in the zigzag direction (see Fig. 2). A small imaginary part $\varepsilon = 10^{-5}$ eV is added to the energy for numerical stability. If the spins are decoupled in the leads, it is easy to demonstrate that the spin-channel resolved transmittance between the leads of a spin-dependent two-terminal system becomes [19,32]

$$T_{\sigma,\sigma'} = \text{Tr}\{\Gamma_\sigma^{(L)} G \Gamma_{\sigma'}^{(R)} G^\dagger\}, \quad (5)$$

where $\Gamma_\sigma^{(L)}$ ($\Gamma_{\sigma'}^{(R)}$) is the linewidth function of the left (right) lead with spin σ (σ'). The transmittance on this form can be computed efficiently using the recursive Green's functions (RGF) technique (as outlined in Refs. [25,33]). All calculations are performed on unit cells with a relatively large width of

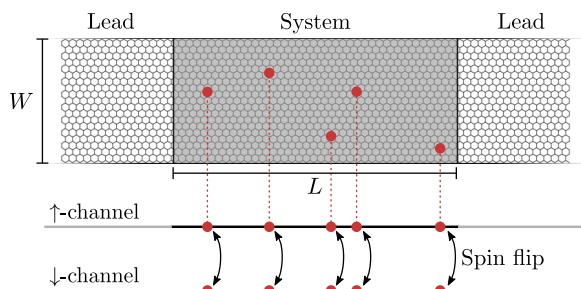


FIG. 2. (Color online) Unit cell of width W and length L as used in the simulations. The unit cell is repeated periodically transverse to the leads. The spin-dependent transport is equivalent to having two separate channels that couple only at magnetic impurity sites.

12.8 nm in order to minimize finite size effects. Furthermore, the calculations are performed using periodic boundary conditions transverse to the transport direction and the results are averaged over 29 k points. Exactly at the charge neutrality point (CNP), the only propagating mode in the leads is at $k = 0$ and it is therefore important to ensure that this is included.

The spin-conserved transport is defined as $T_{sc} = T_{\uparrow\uparrow} + T_{\downarrow\downarrow}$ and the spin-flipped transport is defined as $T_{sf} = T_{\uparrow\downarrow} + T_{\downarrow\uparrow}$. We expect the total transport $T = T_{sc} + T_{sf}$ to be either Ohmic or localized. For Ohmic transport the resistance per unit cell is $R(L) = R_c + R_s L/W$, where R_c is the contact resistance, R_s is the sheet resistance, L is the device length, and W is the width of the unit cell. In the localization regime, the resistance is $R(L) = R_c \exp(L/\xi)$, where ξ is the localization length. By fitting the total transport to a compound expression

$$R(L) = \frac{h}{2e^2 T} = R_c \exp(L/\xi) + R_s L/W, \quad (6)$$

we obtain both localization length and Ohmic resistance. In the limits $\xi \rightarrow \infty$ and $R_s \rightarrow 0$, this expression reduces to the Ohmic and localization regimes, respectively.

We can use the spin polarization P to obtain the spin relaxation length λ_s . According to Zurek *et al.* [20], the spin relaxation mechanism can be either exponential or Gaussian, depending on the distribution of spin couplings to an environment. In order to include both cases as well as any intermediate relaxation mechanism, we fit the output spin polarization of a device with length L according to the following expression,

$$P(L) = \frac{T_{sc}(L) - T_{sf}(L)}{T_{sc}(L) + T_{sf}(L)} = e^{-(L/\lambda_s)^n}. \quad (7)$$

It follows that the spin relaxation behavior is exponential when $n = 1$ and Gaussian when $n = 2$.

III. RESULTS

The output spin polarization of a system containing a single H adatom is shown in Fig. 3. When there is only a single defect, the transport properties do not depend on

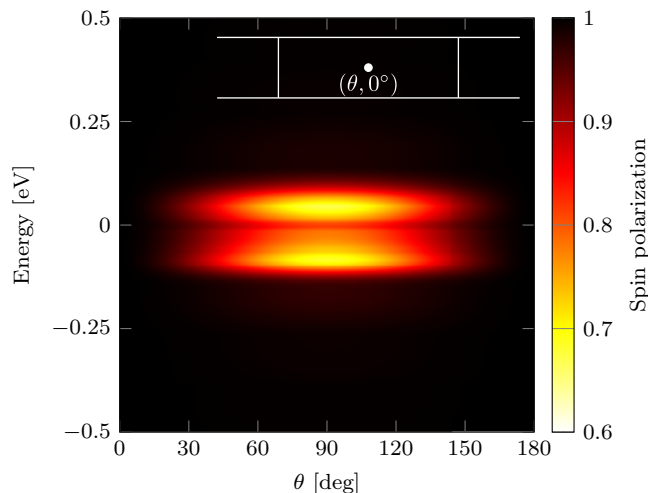


FIG. 3. (Color online) Spin polarization as a function of energy and angle of a graphene system with a single H adatom. The inset shows an illustration of the device.

the azimuthal defect spin angle ϕ . Therefore, only the polar angle θ and the energy E are varied. The figure shows that the spin scatters very strongly near the CNP, $E \simeq 0$, resulting in a significantly decreased spin polarization. This is a consequence of scattering on H adatoms, which have defect bands that span approximately ± 0.1 eV around the CNP (cf. Fig. 1). This means that a single H adatom with defect spin perpendicular to the charge carrier spin is able to destroy almost half of the spin polarization for energies near the CNP. This is in good agreement with Wilhelm *et al.* [19], who found that an $N = 11$ armchair graphene nanoribbon with a single H adatom can have spin-flip transmittance that can surpass the spin-conserved part.

In order to obtain information on the interference effects on spin flipping, we calculate the output spin polarization of a system with two H adatoms separated by a distance of 2.21 nm parallel to the transport direction [see Fig. 4(b)]. The output spin polarization is evaluated at the CNP and the orientations of the defect spins have been chosen to be $(\theta_1, \phi_1) = (90^\circ, 0^\circ)$ and (θ_2, ϕ_2) , respectively. The figure shows that the output spin polarization is minimal when the defect spins are perpendicular to the charge carrier spin and point in the same direction, whereas it is maximal, when the spins are perpendicular to the charge carrier spin and point in opposite directions. In Fig. 3, we saw that a single defect with spin perpendicular to the charge carrier spin could flip almost half of the electron spin to the opposite channel. Now we see that by having two defects with oppositely oriented spins, the second can almost completely negate the first spin flip. When the two defect spins point in opposite directions, the phase change associated with spin flipping will have equal size and opposite sign. This means that the electron spin will be in phase with the charge carrier spin after the second spin flip, leading to constructive interference. This is not necessarily the case when the defect spins point in the same direction. The interference between defects is thus very important and should not be ignored. Furthermore, the spin-scattering strength depends strongly on the relative position of the two defects,

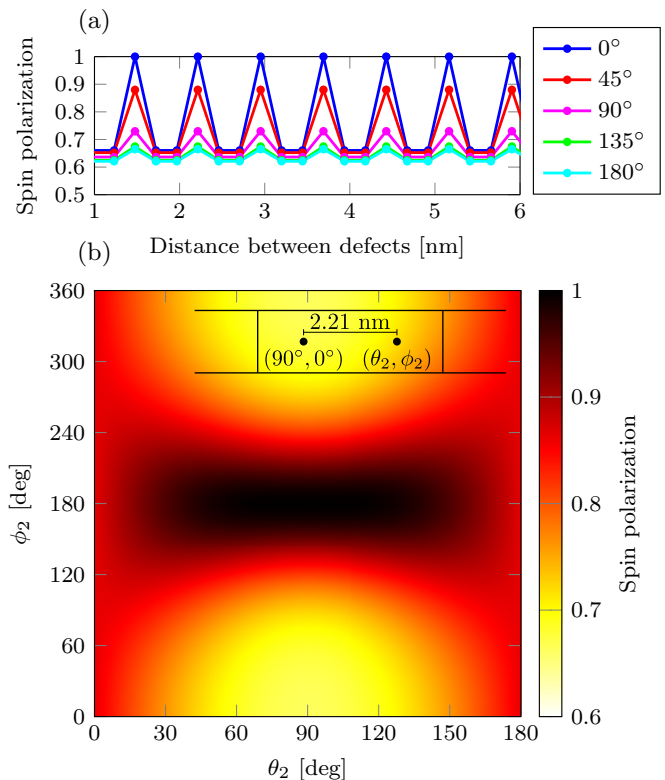


FIG. 4. (Color online) Spin polarization of a system with two H adatoms at an energy of $E = 0.0$ eV. The H adatoms are placed on a line parallel to the transport direction and the defect spin angles are $(\theta_1, \phi_1) = (90^\circ, 0^\circ)$ and (θ_2, ϕ_2) , respectively. (a) The distance between the defect is varied and θ_2 has been fixed to 90° . (b) The defects are placed 2.21 nm apart.

which is illustrated in Fig. 4(a), where the spin polarization is calculated as a function of distance between them. The figure shows that at the CNP, the output spin polarization is periodic with the distance between them with a period of three graphene lattice constants. Presumably, the periodicity arises due to the same quantization phenomenon that causes every third armchair graphene nanoribbon to be metallic, and the remaining nanoribbons to be semiconducting.

We now turn to calculating the effects of multiple magnetic hydrogen adatoms on graphene. We place hydrogen adatoms at random positions uniformly distributed across the device according to a predefined impurity concentration η . We wish to keep the device nonmagnetic in order to isolate spin relaxation from other magnetic effects. Therefore, we choose the directions of the defect spins at random, uniformly distributed on a Bloch sphere. The transport is calculated for very long devices of 147.5 nm, which contain a total of 72 000 carbon atoms in the unit cell. Using the RGF method, we can extract the transport after each slice of the device, allowing us to obtain the transport results for all device lengths until the chosen maximum length. In order to minimize the effects of the finite width of the unit cell, we average over an ensemble of 150 device realizations. The spin polarization as a function of device length and energy for different impurity concentrations is shown in Fig. 5 as well as an example of transmittance and spin polarization as a function of device

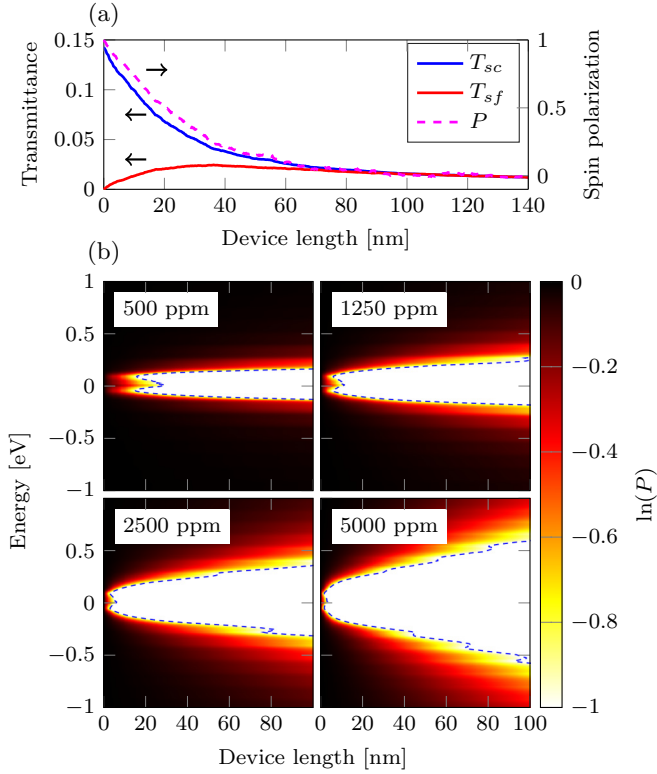


FIG. 5. (Color online) (a) Ensemble-averaged transmittance and spin polarization as a function of device length for a system with impurity concentration $\eta = 500$ ppm calculated at the CNP. (b) Ensemble-averaged spin polarization as a function of energy and device length for different impurity concentrations. The dashed lines show the spin relaxation length.

length for a single energy and impurity concentration. We show the logarithm of the spin polarization in the range between -1 and 0 in order to highlight the spin relaxation length, which is defined as the device length at which $\ln[P(L)] = -1$. The figure shows that the spin polarization decays very fast for energies close to the H adatom defect bands (cf. Fig. 1). As expected, the spin polarization decays faster with increasing impurity concentration. Note that the spin polarization also decays for energies away from the H defect bands, due to the relatively small, but finite, spin splitting in the remaining band structure. The small energy-dependent oscillations in Figs. 5 and 6 are due to finite size effects originating from the finite width of the unit cell.

Equation (7) with two fitted parameters captures the simulated spin polarization as a function of device length very accurately. The fitted parameters are the spin relaxation length λ_S as well as the exponent n , which provides information on the spin relaxation mechanism [see Fig. 6(a)]. A few examples of the fitting procedure are included in Fig. 6(b) in order to illustrate the excellent quality of the fits. The carrier concentration in the figure is computed at Fermi energies corresponding to the energy axis. Positive and negative carrier densities refer to electron and hole doping, respectively. The spin relaxation length is very short for energies near the H defect bands. For the same energies, the spin relaxation mechanism is predominantly exponential with an exponent

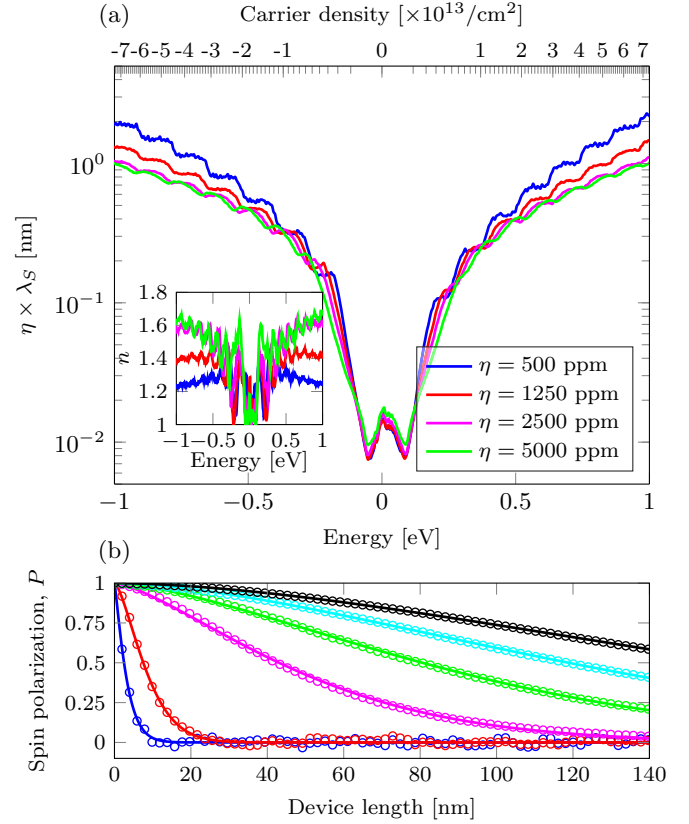


FIG. 6. (Color online) (a) Normalized spin relaxation length $\eta \times \lambda_S$ and exponent n (inset) obtained by fitting against Eq. (7). The spin relaxation lengths are normalized with the defect concentration in order to illustrate that their inverse scale nearly linearly with respect to it. (b) Examples of fitting the spin relaxation against Eq. (7) of a system with 5000 ppm H adatoms for different energies. The energies are between 0.0 eV (fastest decay) and 1.0 eV (slowest decay) in steps of 0.2 eV. The circles are the ensemble averaged spin polarizations and the lines are the corresponding fitted functions. For visualization purposes, only every fourth data point is shown.

of $n \simeq 1$. For energies further away from the CNP, the spin relaxation length increases. We note that λ_S has two minima near the CNP, which are correlated with the large spin splitting of the H adatom defect bands. Exactly at the CNP, the spin splitting of the defect bands is vanishing, resulting in a local maxima. The figure shows that there is an almost linear scaling of the inverse spin relaxation length λ_S^{-1} with respect to impurity concentration η , especially near the CNP. Away from the CNP we observe that n decreases with decreasing impurity concentration. This suggests that the spin relaxation mechanism tends toward exponential (Markovian) behavior in the highly dilute impurity limit. Importantly, we see that the decay of the spin polarization as a function of device length need not be exponential nor Gaussian, which means that a more complete theory on spin relaxation should not presume anything about the spin relaxation behavior, except in the limit of very dilute systems, where the approximation of exponential decay seems to be valid. For energies near the CNP, the normalized localization length is $\eta \times \lambda_S \approx 0.01$ nm. In order to obtain experimentally observed spin relaxation length of about $\lambda_S \simeq 2 \mu\text{m}$ [3], the impurity concentration should be

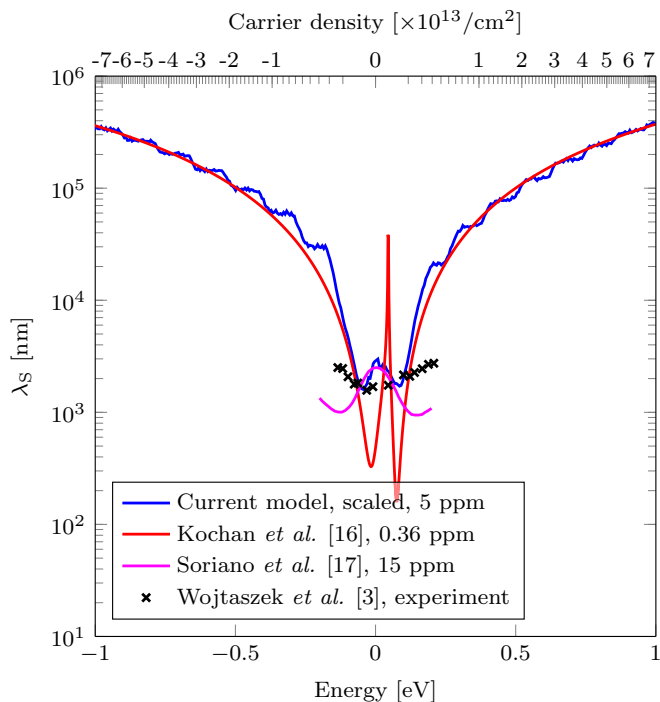


FIG. 7. (Color online) Comparison of spin relaxation lengths obtained by different authors.

$\eta \approx 5$ ppm, which is more than an order of magnitude larger than the prediction by Kochan *et al.* [16] of 0.36 ppm. We expect our model to be more accurate as it is based on a full transport calculation and therefore takes interference effects into account. Our prediction of the impurity concentration is, however, in closer agreement with Soriano *et al.* [18], who found that an impurity concentration of 15 ppm gives spin relaxation times in agreement with an experiment based on time propagation of the spin polarization operator using a self-consistent Hubbard model.

A comparison of spin relaxation lengths obtained by the current model and those obtained by other theoretical methods and experiments is presented in Fig. 7. We have scaled our 500 ppm result to 5 ppm by multiplying it by a factor of 100. The two other theoretical methods [16,17] give the spin relaxation time τ_S , which is related to the spin relaxation length by $\lambda_S = v_S \tau_S$ in the ballistic regime and by $\lambda_S = \sqrt{D_S \tau_S}$ in the diffusive regime, where v_S is spin carrier velocity and D_S is the spin diffusion constant. In the low-defect-density case, we expect to be in the ballistic regime. Therefore, we compare results that are all obtained in the low-defect-density case. We obtain a velocity $v_S = 1.65 \times 10^4$ m/s by a least squares fitting between our result and the analytic result obtained by Kochan *et al.* [16]. We observe that the result by Kochan *et al.* is in fairly good agreement with ours regarding the location of the two minima near the CNP and in quantitative agreement further away from the CNP. However, their result predicts variations over several orders of magnitude near the CNP, whereas our result predicts a variation of only about a factor of 2. In fact, their result is singular exactly at the CNP, because it is neither broadened by the self-energy due to leads or by finite geometry effects.

Furthermore, we compare with the experimental results of hydrogenated graphene obtained by Wojtaszek *et al.* [3]. Note that the experimental results were obtained without detailed knowledge of the defect concentration. However, the authors estimated the concentration to be around 200 ppm. Lastly, we compare our results to the theoretical result by Soriano *et al.* [17]. The figure shows that their result is neither in qualitative agreement with our model nor the analytic result by Kochan *et al.* or experiment. We speculate that the deviation arises from the fact that Soriano *et al.* uses vacancies in graphene to model hydrogen adatoms, whereas both our model and the model used by Kochan *et al.* employ a parametrization of hydrogen on graphene. Theoretical predictions [16,18,34], including our own, show that the spin relaxation time (or spin relaxation length) decreases with increasing impurity concentration. However, experimental work on hydrogenated graphene shows that the spin relaxation time (or spin relaxation length) actually increases with increasing impurity concentration [3]. The origin of this discrepancy remains elusive, but could stem from interactions between graphene and the substrate, as this has not been included in any of the theoretical models. Another possibility is that the hydrogen plasma used in the experiments was additionally cleaning the graphene surface, thus increasing the spin relaxation time. Finally, a recent paper by Idzuchi *et al.* [35] discusses the possibility that details of the Hanle measurements were not taken into account in the data analysis.

By fitting the total transmittance against Eq. (6) we obtain the Ohmic sheet resistance as well as the localization length

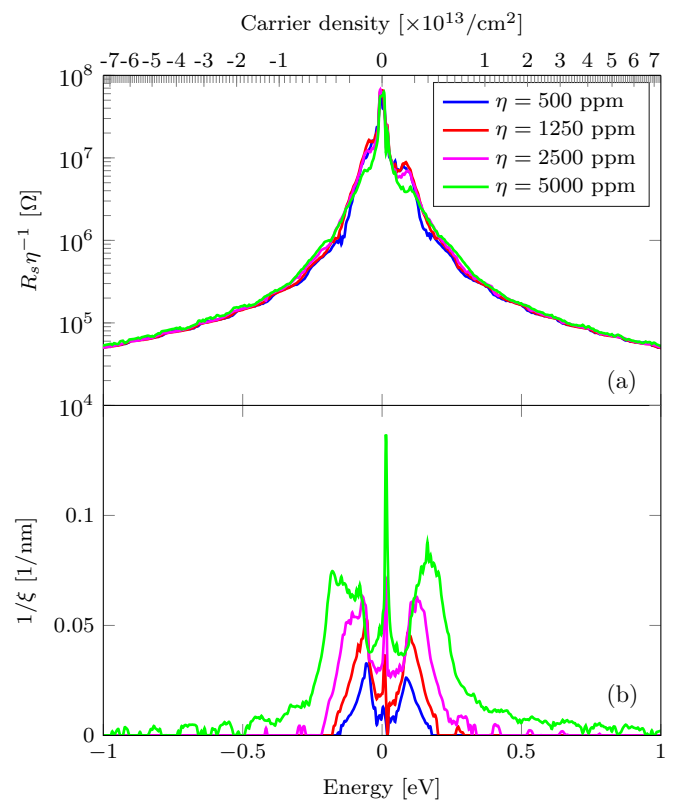


FIG. 8. (Color online) (a) Normalized Ohmic sheet resistance R_s/η and (b) inverse localization length $1/\xi$ obtained by fitting against Eq. (6).

(see Fig. 8). We observe localization near the H defect bands (cf. Fig. 1) and vanishing localization elsewhere. Additionally, the figure shows that the sheet resistance scales linearly with respect to impurity concentration. However, the scaling of the localization length is far from linear, which shows that the induced localization per atom decreases with increasing impurity concentration. Furthermore, as the impurity concentration is decreased, the energy window at which there is localization, narrows.

IV. CONCLUSIONS

In this work, we study spin-dependent transport of hydrogenated graphene. We use a simple model with only a spin-dependent on-site potential at the defect site to describe hydrogen adatoms on graphene. As the model is simple, some of the results are expected to extend qualitatively to other systems as well. We have demonstrated that the Landauer-Büttiker formalism can be used to calculate spin-dependent transport of systems with magnetic impurities with individually oriented magnetic moments. In this work, we study hydrogen adatoms on graphene. By calculating the spin-dependent transport as a function of device length, we can extract properties such as spin relaxation length, localization length, and sheet resistance. We have shown that there is strong localization for energies

around the hydrogen-induced defect bands, which also lead to a very high sheet resistance. Away from the defect bands there is vanishing localization. Furthermore, we have demonstrated that the spin relaxation length is very short for energies around the hydrogen-induced defect bands and that the spin relaxation mechanism is exponential (Markovian) near the CNP and nonexponential (non-Markovian) otherwise. Additionally, we have shown that the inverse spin relaxation length and sheet resistance scale nearly linearly with impurity concentration, whereas the localization length does not.

ACKNOWLEDGMENTS

M.R.T. and T.G.P. gratefully acknowledge the financial support from the Center for Nanostructured Graphene (Project No. DNR58) financed by the Danish National Research Foundation and from the QUSCOPE project financed by the Villum Foundation. The work by A.H. and M.M.E. has been supported by the Academy of Finland through its Centres of Excellence Program (Project No. 251748). We acknowledge the computational resources provided by Aalto Science-IT project and Finland's IT Center for Science (CSC). M.M.E. acknowledges financial support from the Finnish Cultural Foundation.

-
- [1] D. Huertas-Hernando, F. Guinea, and A. Brataas, *Phys. Rev. Lett.* **103**, 146801 (2009).
- [2] W. Han, R. K. Kawakami, M. Gmitra, and J. Fabian, *Nat. Nanotechnol.* **9**, 794 (2014).
- [3] M. Wojtaszek, I. J. Vera-Marun, T. Maassen, and B. J. van Wees, *Phys. Rev. B* **87**, 081402 (2013).
- [4] N. Tombros, S. Tanabe, A. Veligura, C. Jozsa, M. Popinciuc, H. T. Jonkman, and B. J. van Wees, *Phys. Rev. Lett.* **101**, 046601 (2008).
- [5] N. Tombros, C. Jozsa, M. Popinciuc, H. T. Jonkman, and B. J. van Wees, *Nature (London)* **448**, 571 (2007).
- [6] W. Han and R. K. Kawakami, *Phys. Rev. Lett.* **107**, 047207 (2011).
- [7] M. Wojtaszek, I. J. Vera-Marun, E. Whiteway, M. Hilke, and B. J. van Wees, *Phys. Rev. B* **89**, 035417 (2014).
- [8] P. J. Zomer, M. H. D. Guimarães, N. Tombros, and B. J. van Wees, *Phys. Rev. B* **86**, 161416 (2012).
- [9] B. Dlubak, M.-B. Martin, C. Deranlot, B. Servet, S. Xavier, R. Mattana, M. Sprinkle, C. Berger, W. A. De Heer, F. Petroff, A. Anane, P. Seneor, and A. Fert, *Nat. Phys.* **8**, 557 (2012).
- [10] M. H. D. Guimarães, P. J. Zomer, J. Ingla-Aynés, J. C. Brant, N. Tombros, and B. J. van Wees, *Phys. Rev. Lett.* **113**, 086602 (2014).
- [11] S. Lara-Avila, S. Kubatkin, O. Kashuba, J. A. Folk, S. Lüscher, R. Yakimova, T. J. B. M. Janssen, A. Tzalenchuk, and V. Fal'ko, *Phys. Rev. Lett.* **115**, 106602 (2015).
- [12] O. V. Yazyev and L. Helm, *Phys. Rev. B* **75**, 125408 (2007).
- [13] Y. Ma, P. O. Lehtinen, A. S. Foster, and R. M. Nieminen, *New J. Phys.* **6**, 68 (2004).
- [14] A. V. Krasheninnikov, P. O. Lehtinen, A. S. Foster, P. Pyykkö, and R. M. Nieminen, *Phys. Rev. Lett.* **102**, 126807 (2009).
- [15] M. R. Thomsen, S. J. Brun, and T. G. Pedersen, *Phys. Rev. B* **91**, 125439 (2015).
- [16] D. Kochan, M. Gmitra, and J. Fabian, *Phys. Rev. Lett.* **112**, 116602 (2014).
- [17] D. Soriano, N. Leconte, P. Ordejón, J.-C. Charlier, J.-J. Palacios, and S. Roche, *Phys. Rev. Lett.* **107**, 016602 (2011).
- [18] D. Soriano, D. Van Tuan, S. M. Dubois, M. Gmitra, A. W. Cummings, D. Kochan, F. Ortmann, J.-C. Charlier, J. Fabian, and S. Roche, *2D Mater.* **2**, 022002 (2015).
- [19] J. Wilhelm, M. Walz, and F. Evers, *Phys. Rev. B* **92**, 014405 (2015).
- [20] W. H. Zurek, F. M. Cucchiatti, and J. P. Paz, *Acta Phys. Pol., B* **38**, 1685 (2007).
- [21] W. A. Coish, J. Fischer, and D. Loss, *Phys. Rev. B* **77**, 125329 (2008).
- [22] S. R. Power and A.-P. Jauho, *Phys. Rev. B* **90**, 115408 (2014).
- [23] M. R. Thomsen, S. J. Brun, and T. G. Pedersen, *J. Phys.: Condens. Matter* **26**, 335301 (2014).
- [24] S. Datta, *Electronic Transport in Mesoscopic Systems* (Cambridge University Press, Cambridge, UK, 1995).
- [25] T. Markussen, R. Rurali, M. Brandbyge, and A.-P. Jauho, *Phys. Rev. B* **74**, 245313 (2006).
- [26] T. G. Pedersen and J. G. Pedersen, *J. Appl. Phys.* **112**, 113715 (2012).
- [27] J. G. Pedersen, T. Gunst, T. Markussen, and T. G. Pedersen, *Phys. Rev. B* **86**, 245410 (2012).
- [28] R. Balog, B. Jørgensen, L. Nilsson, M. Andersen, E. Rienks, M. Bianchi, M. Fanetti, E. Lægsgaard, A. Baraldi, S. Lizzit, Z. Sljivancanin, F. Besenbacher, B. Hammer, T. G. Pedersen, P. Hofman, and L. Hornekær, *Nat. Mater.* **9**, 315 (2010).

- [29] V. Blum, R. Gehrke, F. Hanke, P. Havu, V. Havu, X. Ren, K. Reuter, and M. Scheffler, *Comput. Phys. Commun.* **180**, 2175 (2009).
- [30] J. P. Perdew, K. Burke, and M. Ernzerhof, *Phys. Rev. Lett.* **77**, 3865 (1996).
- [31] Y. Hancock, A. Uppstu, K. Saloritta, A. Harju, and M. J. Puska, *Phys. Rev. B* **81**, 245402 (2010).
- [32] T. P. Pareek and P. Bruno, *Phys. Rev. B* **65**, 241305 (2002).
- [33] A. MacKinnon, *Z. Phys. B* **59**, 385 (1985).
- [34] D. Van Tuan, F. Ortmann, D. Soriano, S. O. Valenzuela, and S. Roche, *Nat. Phys.* **10**, 857 (2014).
- [35] H. Idzuchi, A. Fert, and Y. Otani, *Phys. Rev. B* **91**, 241407 (2015).